HEVEN: Small Object Search and Navigation on VLM-Based Autonomous Mobile Systems

ABSTRACT

Autonomous mobile systems such as service robots are increasingly deployed across homes, offices, and healthcare facilities for diverse service tasks. A particularly important yet challenging capability is helping users search for and navigate to small daily objects such as keys and medications, which are numerous, frequently relocated, and difficult to detect in cluttered environments. An emerging paradigm leverages cloud-based vision-language models (VLMs) for this task, but existing approaches suffer significant performance degradation when the target shifts from large, stationary furniture to small movable objects. We propose HEVEN, the first VLM-based autonomous mobile system that enables accurate and efficient small object search and navigation. In particular, the key idea of HEVEN is to organize scene memory hierarchically based on spatial containment and support relationships. HEVEN constructs a spatial semantic tree (SST) that organizes navigation targets into three spatial levels based on containment and support relationships. To locate and navigate to the target, HEVEN queries the cloud-based VLM hierarchically on the SST to narrow the search space, and guides the mobile system to verify candidates while accounting for travel cost. Moreover, HEVEN pipelines VLM reasoning with physical control, keeping the mobile system in continuous movement as navigation targets are progressively refined. Extensive experiments on two new datasets we collect, spanning 10 real-world and 100 synthetic scenes with over 3, 100 episodes, show that HEVEN achieves over 74% success rate, outperforming state-of-the-art (SOTA) baselines by over 40% with 4× higher path efficiency. HEVEN also reduces the memory footprint by 8.7× and the VLM inference overhead by 4.4× compared to the SOTA baselines.

1 INTRODUCTION

Autonomous mobile systems, such as service robots [26, 56, 16, 9] and autonomous vehicles [50, 11, 66], are experiencing rapid adoption across homes, offices, healthcare facilities, and public venues, with the global service robotics market projected to exceed 100 billion by 2030 [18]. While these systems support diverse tasks ranging from delivery [59, 21] to inventory management [10], a particularly high-demand capability is helping users search for and retrieve small daily objects [6, 30] such as keys, eyeglasses, and medications. Studies estimate that people spend approximately 10 minutes per day searching for misplaced items [39]. This burden is particularly acute for elderly individuals and those with cognitive impairments, for whom misplacing belongings is far more frequent and unassisted searching can lead to distress and injuries [1, 40]. However, small object search and navigation presents unique challenges compared to large, stationary furniture (*e.g.*, sofas or refrigerators) whose positions are stable and can be pre-mapped. A typical household contains thousands of small movable items [3], many of which are relocated multiple times daily. Their small physical size makes them difficult to detect and easily occluded in cluttered environments, rendering both visual recognition and spatial reasoning particularly challenging. Traditional navigation approaches [51, 33, 20, 4] that rely on static geometric maps (*e.g.*, occupancy grids built via SLAM) cannot accommodate such dynamic, semantics-driven search tasks.

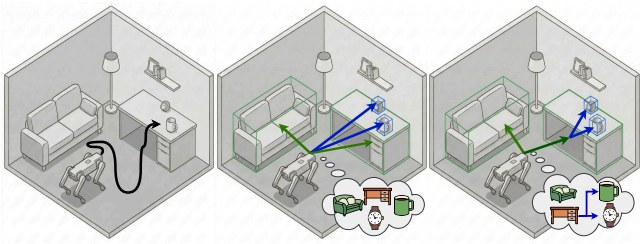

Figure 1: VLM-based object search and navigation methods: (a) non-memory approaches resort to blind search; (b) existing memory-based approaches present an unstructured flat memory to the VLM, resulting in high reasoning errors; (c) HEVEN organizes scene memory hierarchically based on spatial containment and support relationships.

Recent research suggests to leverage vision-language models (VLMs) [70, 32, 29, 62, 61], which combine visual perception with semantic reasoning, to search for and navigate to objects without requiring pre-built geometric maps or known target coordinates. Some works [64, 68] fine-tune VLMs on navigation-specific datasets to allow direct outputs of navigation actions, but collecting sufficient training data for diverse environments is costly and the fine-tuned models often generalize poorly to unseen scenes [49, 62]. In contrast, a better alternative is *zero-shot* VLM-based navigation, which uses pre-trained VLMs without task-specific fine-tuning. A naive method is to query a cloud-based VLM with a target description or reference image [62, 61], together with real-time sensor observations, to make navigation decisions. However, without having memory of the environment, these methods resort to blind search and are prone to redundant

exploration (see Fig. 1a). Other methods [60, 58] construct a *flat scene memory* as an unstructured collection of geo-tagged images or detected objects with depth information, and present it to the VLM to identify possible target locations (see Fig. 1b). While these methods enable more targeted navigation, their performance degrades sharply as the target object becomes smaller. Our case study (Sec. 2) shows that for small movable targets (*e.g.*, a watch), the success rates of SOTA non-memory and memory-based navigation methods drop by up to 55% and 70% respectively, compared to their performance on large targets (*e.g.*, a sofa).

From these observations, our key insight is that scene memory in the form of spatially-structured visual inputs with depth information, is critical for VLM-based autonomous mobile systems to locate small movable objects. However, organizing and querying the memory as a flat and unstructured collection of images or detection results is neither effective nor efficient. In this paper, we instead propose to *organize scene memory **hierarchically** based on spatial containment and support relationships* (see Fig. 1c). This rationale stems from how humans remember object locations: rather than memorizing exact coordinates, they associate objects with the spaces and entities that contain or support them (*e.g.*, a cup is on the dining table, which is in the kitchen). By encoding these relationships, a hierarchical memory naturally decomposes the object search into progressive levels, guiding the VLM to reason from broad regions (*e.g.*, which room) to specific destinations (*e.g.*, which table). This coarse-to-fine reasoning enables the VLM to more effectively infer possible locations of small movable objects through their spatial context, while efficiently narrowing the candidate set at each level to reduce inference cost. In Sec. 2, we use a simple case study to show that, even a naive implementation of hierarchical memory outperforms its flat-memory counterpart in both success rate and search time, and the improvement is particularly significant for small targets (i.e., 20% improvement on success rate).

Based on this idea, we present HEVEN, the first Hierarchical mEmory for VLM-Enhanced Navigation system that enables the autonomous mobile system to collaborate with the cloud-based VLM for accurate and efficient small object search and navigation. HEVEN consists of the following three key components. First, it constructs and maintains a *spatial semantic tree* (SST) as the hierarchical scene memory, which organizes navigation targets into three spatial levels based on containment and support relationships. In particular, we introduce the pillar abstraction to anchor a group of small objects to the entity that supports them, forming a compact navigable unit. Second, the *tree-of-thought (ToT) reasoning engine* operates on the SST in two coordinated phases during object search and navigation: a logical pruning phase that queries the cloud-based VLM to hierarchically narrow down the search space, and a physical traversal phase that guides the mobile system to verify the remaining candidate targets. Lastly, the *asynchronous speculative execution module* progressively refines navigation targets as each level of pruning completes, with a decoupled planner-controller architecture that prevents the mobile system's navigation actions from being delayed by longhaul VLM reasoning.

HEVEN offers several key advantages: (1) The hierarchical structure of SST enables the VLM to reason over a small set of candidate targets at each spatial level rather than the entire memory, hence significantly reduces the reasoning errors and inference cost. (2) The pillar abstraction anchors small movable objects to stable entities, so that navigation targets become robust structural landmarks rather than individual items. (3) The ToT reasoning engine jointly optimizes semantic relevance and physical-world motion cost in navigation, hence largely reduces the path length. (4) The asynchronous speculative execution pipelines cloud VLM inference with mobile system control, enabling the system to navigate toward coarse destinations while finer-grained targets are being resolved by the VLM, effectively masking the cloud's compute latency behind the mobile system's movement.

Since existing navigation benchmarks [12] primarily target large, static furniture, we collect two new datasets for small daily object search and navigation evaluation: a real-world dataset of 600 episodes across 10 scenes using a Unitree Go2 quadruped [53], and a synthetic dataset of 2,500 episodes across 100 procedurally generated scenes using Infinigen [42] and NVIDIA IsaacSim [36]. Our extensive experiments show that HEVEN achieves 77.17% and 73.86% object search and navigation success rate on the real-world and synthetic datasets, respectively, over 40% higher than the SOTA baselines. HEVEN also exhibits 4× higher path efficiency with 22% less end-to-end search time. HEVEN requires only 15.8 MB for SST storage, an 8.7× reduction compared to flat memory methods. Moreover, HEVEN consumes $7.22k$ tokens and 16.4 s of VLM inference time per reasoning task, reducing the inference overhead by 2.4× and 4.4× compared to the non-memory and memory-based baselines, respectively.

2 MOTIVATION STUDY

We conduct a measurement study of the existing VLM-based navigation approaches (Sec. 2.1 and Sec. 2.2) to get the key insights into the advantages of hierarchically organizing the scene memory for navigation (Sec. 2.3).

Measurement Setup. We conduct the measurement study using a scene generated by Infinigen [42], which is widely used for procedural 3D scene generation. Specifically, we generate a $20\,m \times 20\,m$ apartment with 7 rooms and various objects ranging from large furniture such as beds, sofas, and tables to small everyday items such as bags, watches, and

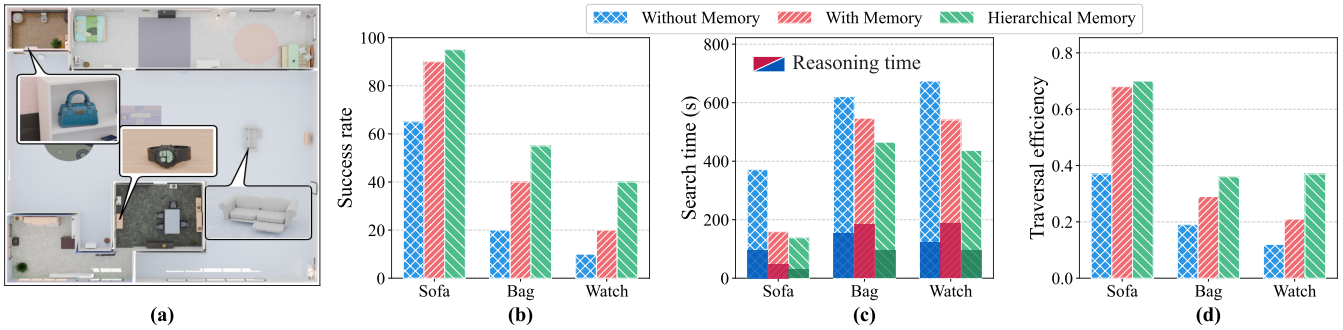

Figure 2: A motivation case study. (a) The simulated apartment scene and the target objects; (b) Success rate comparison; (c) End-to-end search time comparison; (d) Traversal efficiency comparison, which is denoted by the ratio of the shortest path to the actual traversal path in successful cases.

cups (see Fig. 2a). We import it into NVIDIA Isaac Sim [36] to conduct navigation experiments. We implement three methods for comparison: a state-of-the-art non-memory navigation method [62], a state-of-the-art memory-based navigation method [60], and a naive hierarchical-memory-based navigation method. We measure each method on three target objects of decreasing size (sofa, bag, and watch), with 20 trials per object starting from different initial positions.

2.1 Navigation without Memory

Non-memory navigation approaches [62] leverage the cloud-based VLM to make navigation decisions with detailed target descriptions or a reference image as the query and real-time observations from the onboard sensors. As shown in Fig. 2a and Fig. 2b, the success rate of the non-memory method remains below 70% for all targets and degrades sharply as the object size decreases (*e.g.*, for watch, the success rate drops below 10%, with the majority of trials failing due to timeout). This is because the mobile system relies on real-time onboard perception, and smaller objects are harder to spot in cluttered environments. Without a knowledge memory of the environment, the mobile system has no prior understanding of the scene layout or its contents, rendering a near-blind search. Even in successful cases, the traversal efficiency remains below 0.4 across all targets (Fig. 2c), indicating that the mobile system travels a path significantly longer than the shortest route. These results demonstrate that the absence of environmental memory leads to an inefficient and unreliable search process, particularly for small objects.

2.2 Navigation with Memory

Memory-based navigation approaches [60] construct a memory of the scene and leverage the world knowledge of the cloud-based VLM to reason about the likely location of the target object. As shown in Fig. 2b and Fig. 2c, compared to the non-memory approach, the memory-based method achieves higher success rates and shorter search times, indicating that scene memory enables more targeted navigation. However, its performance still degrades significantly as the object size decreases. A key factor behind this degradation is shown in Fig. 2c: the proportion of time that memory-based method spends for VLM reasoning grows substantially for smaller targets. This is because existing memory-based methods typically organize scene memory as a flat structure, such as a list of geotagged scene images or detected objects [58, 60], and present the entire memory to the VLM in a single query. As the object becomes smaller and harder to distinguish, the VLM has to reason over a large number of candidate targets, which not only inflates inference cost but also increases the risk of hallucination, degrading both efficiency and accuracy. In addition, Fig. 2d shows that the traversal efficiency of the memory-based method remains below 0.5 across all targets. Although the memory enables more targeted navigation, the search strategy does not account for physical travel cost, i.e., the mobile system may strictly follow the VLM's ranking of destinations and traverse back and forth between distant regions, resulting in paths longer than necessary.

2.3 Hierarchical Memory

As discussed in Sec. 2.1 and Sec. 2.2, non-memory navigation resorts to inefficient blind search for small movable objects, while existing memory-based methods, though more targeted, still suffers from VLM hallucination and unnecessary travel due to their flat memory structure. Our key idea to address these limitations is to organize scene memory hierarchically based on spatial containment and support relationships, which stems from how humans naturally understand and recall environments at progressively finer spatial granularity. To validate this idea, we develop a naive hierarchical variant on top of the memory-based method [60]. Specifically, we manually group its scene memory (i.e., a set of geotagged images) by room and select the most representative image for each room. During navigation, the VLM first reasons over the room-level representatives to identify the

most probable room, then reasons over all images within that room to determine the final destination.

As shown in Fig. 2b and Fig. 2c, this naive hierarchical variant consistently improves success rate and reduces search time compared to the existing memory-based method, with the gains more significant for smaller objects. Notably, the time spent on VLM reasoning decreases substantially, as the coarse-to-fine reasoning narrows the candidate set at each level rather than presenting the entire memory at once, reducing both inference cost and hallucination risk. In addition, the hierarchical approach also exhibits higher traversal efficiency (Fig. 2d), as the room-level grouping directs the mobile system to search within a single room before moving to the next, reducing unnecessary back-and-forth travel across distant regions.

Takeaway. The measurement study demonstrates that scene memory is essential for small object navigation, and how it is organized fundamentally affects both navigation accuracy and efficiency. Hierarchical memory based on spatial containment and support relationships enables coarse-to-fine reasoning that reduces VLM inference cost and hallucination risk, while spatially grouping destinations to avoid unnecessary back-and-forth traversal.

3 SYSTEM DESIGN

3.1 System Overview

We propose HEVEN, a novel system that enables the autonomous mobile system to leverage the cloud-based VLM for accurate and efficient small object navigation. Our key idea is to hierarchically organize the environmental memory into a tree structure, where nodes at successive levels represent navigation targets at different spatial scales. HEVEN exploits this hierarchy to efficiently narrow down candidate targets with the VLM and reduce unnecessary travel during navigation. Moreover, this coarse-to-fine decision process allows the mobile system to start navigating toward a coarse destination while the VLM continues refining finer-grained targets, pipelining VLM inference on the cloud with physical control on the mobile system to reduce idle waiting.

As shown in Fig. 3, HEVEN consists of three key components. Firstly, the *spatial semantic tree* (Sec.3.2) is hierarchically constructed and serves as the environmental memory, structuring navigation targets into three spatial levels (i.e., rooms, areas, and pillars) according to their containment and support relationships. In particular, we design a pillar abstraction to anchors a group of small objects to the object that supports them, forming a compact navigable unit that simplifies both VLM reasoning and physical navigation. Then, the *tree-of-thought reasoning engine* (Sec.3.3) operates on the spatial semantic tree in two coordinated phases: a logical pruning phase that queries the cloud-based VLM at each tree level to efficiently narrow the search space, and a physical traversal phase that guides the mobile system to verify remaining candidates while accounting for travel cost. Lastly, the *asynchronous speculative execution* module (Sec. 3.4) addresses the latency mismatch between cloud inference and physical control by progressively refining navigation targets as each level of pruning completes, with a decoupled planner-controller architecture that allows the mobile system to navigate continuously without halting.

3.2 Spatial Semantic Tree

We design the Spatial Semantic Tree (SST) as the knowledge memory for the autonomous mobile system. Unlike existing approaches that typically maintain a flat list of all navigation targets and treat them independently regardless of their spatial scale or physical context, our SST organizes targets of different scales into a hierarchical tree based on real-world containment and support relationships. This tree structure inherently encodes spatial connectivity and traversal cost between targets, enabling efficient navigation with minimal redundant travel. In particular, we group small objects with their vertical supporting entity (*e.g.*, a table and the items on it) into a single minimum navigable unit, which is maintained with a gradual-decay online update strategy to mitigate the impact of small objects' position changes.

3.2.1 SST Architecture. We formalize the SST as a hybrid graph $\mathcal{G} = (\mathcal{V}, \mathcal{E}_{hier} \cup \mathcal{E}_{reach})$. The node set $\mathcal{V}$ represents navigation targets at three spatial scales: $\mathcal{V} = \mathcal{V}_{room} \cup \mathcal{V}_{area} \cup \mathcal{V}_{pillar}$, where hierarchy edges $\mathcal{E}_{hier}$ connect parent and child nodes across adjacent levels to form the backbone, reflecting spatial containment and support relationships.

At the top level, room nodes ($\mathcal{V}_{room}$) represent topologically connected regions (*e.g.*, a kitchen or a living room) and serve as the roots of the tree. Area nodes ($\mathcal{V}_{area}$) partition each room into functional sub-regions based on semantic coherence and physical proximity. Each area node $v_a \in \mathcal{V}_{area}$ and room node $v_r \in \mathcal{V}_{room}$ stores a semantic caption ϕ_v generated by the VLM to summarize the contents of its child nodes. At the leaf level, we introduce *pillar nodes* ($\mathcal{V}_{pillar}$) as the minimum navigable units of the SST. A key challenge in target search is *granularity overload*: when every small object is treated as an independent navigation target, the large number of candidates inflates VLM reasoning cost and increases the risk of hallucination. The pillar addresses this by grouping co-located objects under a shared entity anchor. Specifically, we define each pillar node $v_p \in \mathcal{V}_{pillar}$ as a tuple (e_{key}, O_{mem}), where e_{key} is the key entity (i.e., a stationary piece of furniture such as a table or a shelf) and O_{mem} is the set of member objects physically supported by or contained within it. Each member $o \in O_{mem}$ records an open-vocabulary label l, a 3D bounding box $\mathbf{b}_{3D}$, and a visual

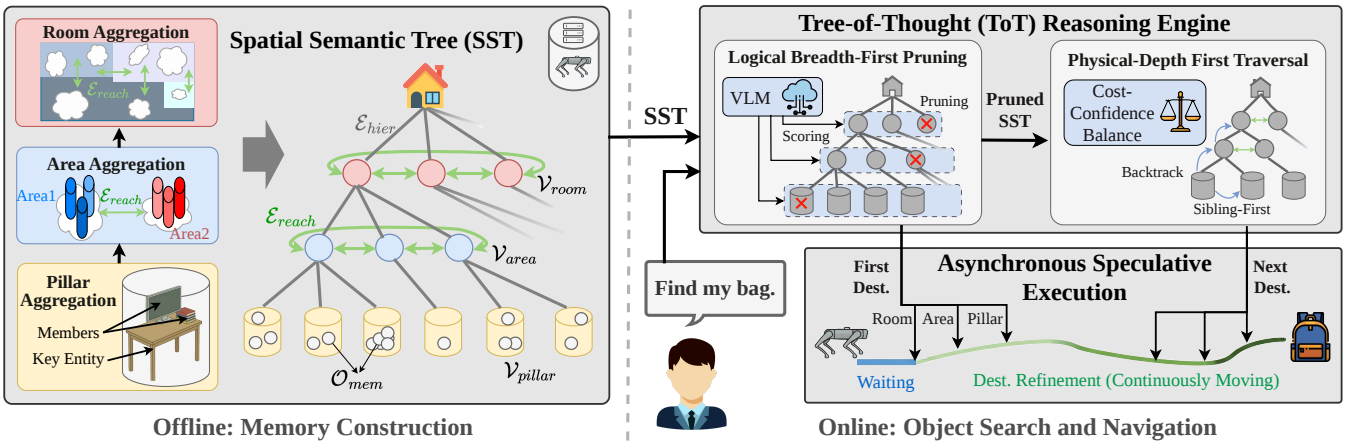

Figure 3: System architecture of HEVEN.

feature embedding [41] $\mathbf{f}_{clip}$. This grouping reduces the number of targets the mobile system and the VLM need to reason about, while the stable entity anchor keeps the navigable unit robust to the scale and positional changes of objects.

Moreover, we add reachability edges $\mathcal{E}_{reach}$ between sibling nodes at the room and area levels to encode spatial connectivity and traversal cost. Each edge $e_{ij} \in \mathcal{E}_{reach}$ is weighted by the geodesic distance $w_{geo}(v_i, v_j)$ on the global map. We omit reachability edges at the pillar level, as pillars within the same area are close enough for the mobile system to assess their geodesic distance and traversability during navigation, and these local metrics may occasionally change (*e.g.*, due to furniture rearrangement). The two types of edges (i.e., $\mathcal{E}_{hier}$ and $\mathcal{E}_{reach}$) play complementary roles in the navigation (Sec. 3.3): the hierarchical tree decomposes the search into level-wise steps, allowing the cloud-based VLM to prune candidates progressively rather than reasoning over the entire flat target set at once; the reachability edges provide traversal cost for path planning, enabling the mobile system to prioritize nearby high-probability targets. The coarse-to-fine structure of SST also naturally supports asynchronous execution between the mobile system and the cloud VLM, as detailed in Sec. 3.4.

3.2.2 Bottom-Up SST Construction. The mobile system explores the environment using a standard frontier-based policy when it first enters an unfamiliar scene[69, 57]. The SST is constructed bottom-up from the sensor data collected during this exploration phase. We employ Grounding SAM [45, 27, 31] as an open-vocabulary detector to process multi-view RGB-D frames and extract the 3D bounding box with a visual feature embedding for each detected object. Observations of the same object from multiple viewpoints are fused based on spatiotemporal consistency, yielding a flat set of distinct detected objects. These objects are then hierarchically assembled into the tree through a two-stage aggregation process.

In the first stage, detected objects $o \in O$ are grouped into pillars based on physical support relationships. A support relationship $o_i \rightarrow o_j$ is identified if o_i physically supports o_j, determined by whether o_j's centroid lies above o_i's top surface within a specified margin and its bird's-eye-view projection falls within o_i's footprint. Objects connected through such relationships are grouped into a pillar v_p, where the root object (i.e., the bottommost supporter, selected by largest base area when ambiguous) becomes the key entity e_{key}, and all objects it supports become its members O_{mem}.

In the second stage, pillar nodes $\mathcal{V}_{pillar}$ are clustered into areas and assigned to rooms. The system computes a pairwise distance between pillars using a metric that combines geodesic proximity and semantic similarity:

$$d_{link}(v_i, v_j) = \alpha \cdot d_{geo}(v_i, v_j) + (1 - \alpha) \cdot (1 - \cos(\mathbf{f}_i, \mathbf{f}_j)), \quad (1)$$

where α is the balance factor. We cluster nearby pillars into area nodes $\mathcal{V}_{area}$ based on this distance metric, and generate a semantic caption ϕ_v for each area by prompting the VLM to summarize its child pillar contents. Room nodes $\mathcal{V}_{room}$ are generated via flood-fill segmentation on the global traversability map. Areas are then assigned to the rooms according to the spatial containment, and a caption is similarly generated for each room by summarizing its area captions. Finally, we establish reachability edges $\mathcal{E}_{reach}$ weighted by geodesic distance between sibling nodes at the room and area levels to complete the full SST graph $\mathcal{G}$.

3.2.3 Continuous SST Update. As small objects in the environment can be frequently added, moved, or taken away, the SST is required to update its memory according to the sensor observations from the mobile system. HEVEN addresses this through a gradual-decay update mechanism. As the mobile system perceives the environment, it compares detected objects against the stored members of nearby pillars. If an object $o \in O_{mem}$ is no longer observed at its recorded position,

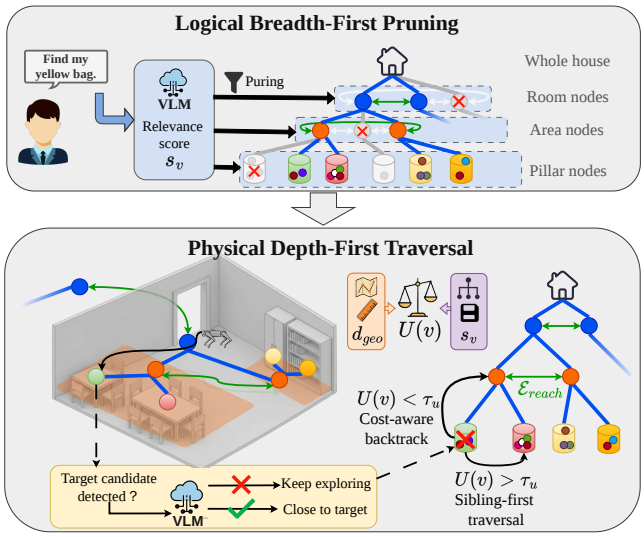

Figure 4: Illustration of tree-of-thought reasoning engine.

the system gradually lowers its confidence score s_o rather than removing it immediately. The object is removed only when s_o falls below a reliability threshold, preventing false deletions caused by temporary sensor occlusion or noise.

Beyond updating small objects in pillars, changes in the environment may require restructuring the tree hierarchy. For instance, when furniture is rearranged across a room, the original area partitioning may no longer reflect the spatial grouping of pillars. However, reconstructing the entire SST at every observation is computationally prohibitive. HEVEN instead triggers local reconstruction only when significant physical changes occur, i.e., when the cumulative displacement of pillar centroids exceeds a distance threshold or the number of pillars changes by a specified percentage. This event-driven approach maintains structural consistency while avoiding unnecessary computation.

3.3 Tree-of-Thought Reasoning Engine

With the SST constructed, the autonomous mobile system has a structured memory of the environment. It is required to determine which of the pillars to visit and in what order during navigation. We design the Tree-of-Thought (ToT) reasoning engine to drive this decision by exploiting the hierarchical structure of the SST and the world knowledge of the cloud-based VLM. As shown in Fig. 4, the engine proceeds in two coordinated phases: (1) a *logical pruning phase* that queries the VLM level by level to efficiently score and eliminate low-probability rooms, areas, and pillars; and (2) a *physical traversal phase* that organizes the remaining candidate pillars into an execution order adapted to the current position and situation of the mobile system.

3.3.1 Logical Breadth-First Pruning. The cloud-based VLM has the world knowledge to reason about where a target object is likely to be found (*e.g.*, a mug is more probably on a kitchen counter than in a hallway). However, directly querying the VLM over all candidate pillars at once is impractical as the large number of unstructured candidates can inflate inference cost and degrade reasoning quality. The hierarchical structure of our SST is well-suited to address this. Rather than presenting the full candidate set, the ToT reasoning engine *queries the VLM level by level*, i.e., starting from rooms, narrowing to areas, and finally to pillars. At each level, the VLM evaluates only the small set of nodes at that level and prunes low-probability branches before expanding to the next level. This progressive breadth-first pruning keeps each VLM query compact and focused, reducing the search space from the entire environment down to a small set of high-probability candidate pillars.

Specifically, upon receiving a navigation query Q, the ToT reasoning engine extracts the target category c_{target} and visual attributes $\mathcal{A}_{vis}$. It then searches top-down through the three levels of the SST, i.e., $\mathcal{V}_{room}$, $\mathcal{V}_{area}$, and $\mathcal{V}_{pillar}$. At the room and area levels, the engine provides the captions ϕ_v of all candidate nodes to the cloud-based VLM, which computes a relevance score $s_v = P_{\text{VLM}}(c_{target} \in v \mid Q, \phi_v)$ for each node reflecting the probability of finding c_{target} there. For each selected parent node, the engine retains the top-k scoring children and expands them as candidates for the next level. At the pillar level, each pillar is provided as the tuple $(e_{key}, \mathcal{O}_{mem})$ and scored by the VLM rather than listing each member object individually, keeping the VLM input compact and grounded in the physical structure of the SST (Sec. 3.2). The pruning terminates at the pillar level as once the mobile system physically reaches a pillar, its onboard sensors can verify the presence of the target within it. This phase outputs a pruned sub-tree retaining up to k children per node. Unlike a flat candidate list, this sub-tree preserves the spatial grouping of candidates where pillars within the same area remain clustered under a parent node.

3.3.2 Physical Depth-First Traversal. Given the pruned sub-tree, our ToT engine first selects the pillar with the highest relevance score (i.e., $\arg\max_v s_v$) as the initial destination. In most scenarios, this high score indicates that the target object was previously detected and recorded in the SST, making the recalled location the most probable place to check first. The mobile system then navigates to this pillar for physical verification. If the target is found, the search concludes. Otherwise, the engine determines subsequent destinations through a hierarchical depth-first process on the pruned sub-tree.

Specifically, when the mobile system verifies a pillar and fails to find the target, the ToT engine sets its relevance score to zero and evaluates the remaining candidate pillars

within the same area. For each unvisited sibling pillar node v, the engine computes a utility score that balances semantic confidence with physical travel cost:

$$U(v) = \frac{s_v}{1 + \lambda \cdot d_{geo}(p_{curr}, v)}, \quad (2)$$

where s_v is the relevance score from the logical pruning phase, $d_{geo}(p_{curr}, v)$ is the geodesic distance from the current pose of the mobile system to pillar v, and λ is a weighting factor. Since the SST does not maintain reachability edges at the pillar level (as mentioned in Sec. 3.2.1), the mobile system estimates d_{geo} locally based on its current observation of the surrounding area. If any remaining pillar has a utility score higher than a threshold (i.e., $U(v) > \tau_u$), the engine selects the one with the highest utility score as the next destination. When no remaining pillar within the current area has a utility score exceeding the threshold, the engine backtracks to the area level and applies the similar utility-based selection (i.e., Eqn. 2) among *sibling areas within the current room*, where d_{geo} in the utility computation is obtained from the reachability edges stored in the SST. If a qualifying area is selected, the engine assigns the pillar with the highest relevance score s_v within that area as the next destination. If no area qualifies either (i.e., the utility scores of all sibling areas are lower than τ_u), the process continues backward to the room level. The hierarchical structure of the pruned sub-tree naturally supports this recursive backtracking as a depth-first traversal: *the ToT engine exhausts spatially proximate, high-probability candidates under the same parent node before incurring the cost of cross-area or cross-room travel.* If the target is not found after traversing the current sub-tree, the engine prunes the visited pillars from the SST and re-initiates the logical breadth-first pruning (Sec. 3.3.1) to produce a new candidate sub-tree for the physical traversal.

In addition, throughout the entire physical traversal, the onboard detector continuously scans the RGB-D stream to check for the target object. Upon detecting a candidate match, the system transmits a cropped image to the cloud-based VLM for confirmation while the mobile system continues its trajectory without stopping. Only a positive VLM confirmation causes the mobile system to interrupt its path for close-range verification. Otherwise, the traversal proceeds without pause. This on-the-move target verification enables temporal overlap between mobile system movement and cloud inference, avoiding unnecessary stops.

3.4 Asynchronous Speculative Execution

As described in Sec. 3.3, upon receiving a navigation query, the ToT engine queries the cloud-based VLM to prune the SST from rooms down to candidate pillars. The full pruning process requires multiple rounds of VLM inference and can take up to tens of seconds. However, room-level pruning completes within seconds as the number of rooms is significantly smaller than that of areas and pillars, and we observe that in the majority of cases the target object is located within the highest-scoring room and area. Therefore, rather than waiting for the entire pruning to finish, HEVEN adopts a speculative execution strategy where the navigation target is progressively refined as each level of pruning is resolved. Once the room-level scoring identifies the most probable room, the mobile system begins traveling toward it. Similarly, when area and pillar-level results become available, the destination is refined to the selected area and pillar. This progressive refinement pipelines VLM inference with physical control, as the hierarchicy of the SST naturally enables reasoning over increasingly precise targets at each level.

To support this progressive refinement without blocking the mobile system's movement, HEVEN decouples the onboard system into a deliberative planner and a reactive controller. The deliberative planner manages communication with the cloud-based VLM and runs the ToT reasoning engine. As each level of pruning completes, the planner pushes the updated navigation target into a thread-safe command queue. The reactive controller operates at high frequency (> 20 Hz), continuously consuming targets from this queue to execute smooth, collision-free movement. When the planner refines the target (i.e., from a room center to an area center, or from an area to a specific pillar), the controller adjusts the trajectory on the fly without halting. This decoupling ensures that the mobile system remains in continuous motion regardless of cloud VLM inference latency.

Table 1: Summary of real-world and synthetic datasets.

Dataset		Scenes	Categories	Objects	Episodes
Real-world		10	6	12	600
Synthetic	Multi-Room	50	10	50	1500
	Single-Room	50	10	50	1000

4 TESTBED AND DATASET

We collect dataset and conduct experiments across real-world and synthetic scenes. We deploy HEVEN on a physical autonomous mobile system to evaluate its end-to-end navigation performance in real-world environments. We further construct procedurally generated synthetic scenes to benchmark specific performance metrics, individual module contributions, and system robustness at a larger scale under controlled scene configurations and object layouts. Tab. 1 summarizes the two datasets.

4.1 Real-World Dataset and Testbed

We collect a real-world dataset across 10 scenes, including homes, offices, dining areas,coffee bars, etc. (see Fig.5), featuring diverse floor plans and functionalities. We select six

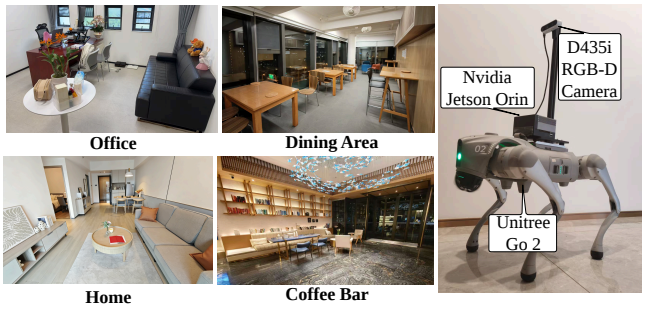

Figure 5: Real-world scenes and testbed.

Figure 6: Examples of synthetic scenes.

target categories grouped into three size classes: large (backpacks, laptops), medium (books, hats), and small (cameras, cellphones), with two visually distinct instances per category, yielding 12 target objects across a total of 600 navigation episodes. This size-based grouping allows us to assess how target physical size affects search performance.

We deploy HEVEN on a Unitree Go2 quadruped [53] equipped with an Intel RealSense D435i depth camera [24] and an NVIDIA Jetson AGX Orin compute module [37]. During operation, the Jetson Orin manages high-frequency local control and perception, while the reasoning is offloaded to a cloud-based VLM (GPT-4o) [38, 67] via API calls.

4.2 Synthetic Dataset

Existing navigation benchmarks (*e.g.*, Matterport3D [12] and Habitat-Matterport 3D [43]) primarily use large, static furniture as navigation targets, which is insufficient for evaluating small movable object search and navigation. We collect a synthetic dataset using Infinigen [42, 54], a procedural 3D scene generator that provides artifact-free meshes, physics-aware object placement, and exact 6-DoF ground truth. The generated scenes are imported into NVIDIA Isaac Sim (Fig. 6) for navigation experiments. We design two benchmarks targeting different evaluation goals.

4.2.1 Multi-Room Benchmark. We generate 50 multi-room scenes (Fig.6a) with diverse layouts to benchmark the object search and navigation performance at scale. Each scene contains 10 target categories, extending the six real-world object categories with four additional small object types (bags, wallets, watches, and keys). To simulate the ambiguity caused by similar objects of the same category, we procedurally place five visually distinct instances per target category in each scene as intra-class distractors, requiring the system to navigate to a specific target instance rather than any object of the same category. We execute a total of 1500 navigation episodes across these environments.

4.2.2 Single-Room Benchmark. We generate 50 single-room scenes (Fig. 6(b)) to stress-test system robustness under controlled scene complexity. We vary two physical dimensions independently: object count and spatial clustering degree. To quantify clustering, we discretize each room into a uniform grid of M cells and compute spatial entropy [7]: $H_s = -\frac{1}{N}\sum_{i=1}^{M} p_i \log p_i$, where N is the total number of objects and p_i is the fraction of objects within the i-th cell. Lower H_s indicates that small objects are concentrated on fewer supporting entities, while higher H_s reflects a more uniform distribution across supporting entities throughout the room. By independently controlling these two dimensions, this benchmark isolates their individual effects on search and navigation performance.

5 EVALUATION

In this section, we conduct extensive experiments to validate the performance and advantages of HEVEN. We first describe the evaluation setup and metrics (Sec. 5.1). We then evaluate the end-to-end performance of HEVEN on the real-world autonomous mobile platform (Sec. 5.2). Next, we benchmark HEVEN against baseline methods on the multi-room synthetic dataset to assess assess navigation accuracy, path efficiency, and search cost across different target sizes (Sec. 5.3). We further stress-test system robustness under varying object counts and spatial clustering using the single-room benchmark (Sec. 5.4). Finally, we conduct ablation studies to quantify the contributions of the hierarchical SST structure and the hybrid search strategy (Sec. 5.5).

5.1 Evaluation Setup and Metrics

Implementation and Setup. We set the number of retained children per node $k = 2$ in the SST pruning to balance VLM reasoning cost and search thoroughness. We empirically set the balance factor α in SST construction to 0.3 and the weighting factor λ in the utility function to 0.1. During evaluation of memory-based methods and HEVEN, we remove all target objects and intra-class distractors during memory construction and reintroduce them during the search phase to prevent the task from degenerating into trivial coordinate recall. In synthetic experiments on NVIDIA Isaac Sim, an episode terminates when the system issues a STOP action

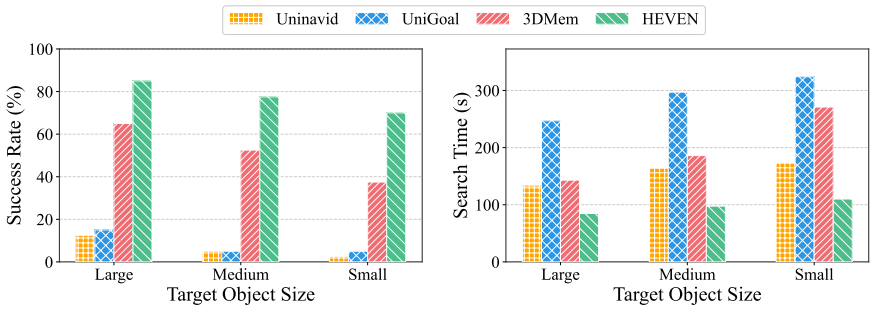

Figure 7: Performance comparison of HEVEN and existing methods on real-world dataset for different target sizes.

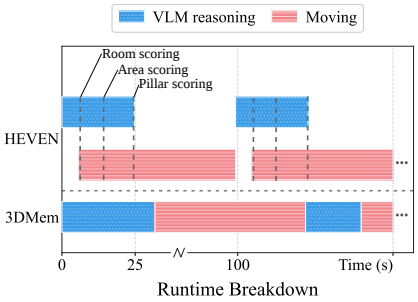

Figure 8: Runtime breakdown comparison of HEVEN and 3DMem.

Table 2: Resource consumption of the memory storage, update, and VLM reasoning. "Mem.","Upd.", and "Inf." denote memory size, update time, and inference time, respectively.

Method	Mem. (MB) ↑	Upd. (min) ↓	Inf. (s) ↓	Tokens ↓
UniGoal [62]	–	–	39.8	12.52k
3DMem [60]	137.2	24.28	73.2	37.28k
HEVEN	**15.8**	**0.58**	**16.4**	**7.22k**

or reaches a 500-step limit, and is considered successful if the system stops within 1.0 m of the correct target instance. Synthetic simulations run on a workstation with an Intel Core i9-14900K CPU and NVIDIA RTX 4090 GPUs.

Metrics. We evaluate performance over N episodes using the following metrics: Success Rate (SR) measures the percentage of episodes where the system successfully locates the target; Success weighted by Path Length [2], SPL $= \frac{1}{N}\sum_{i=1}^{N} S_i \frac{l_i}{\max(p_i,l_i)}$, quantifies path efficiency, where S_i is the success indicator, p_i is the traversed path length, and l_i is the shortest geodesic distance to the target; Distance to Goal (D2G) [6] captures the final proximity error between the stopping position and the target; Steps records the total physical steps per episode; and Category Error [28], CE $= \frac{1}{N}\sum_{i=1}^{N} C_i \times 100\%$, quantifies vulnerability to intra-class distractors, where $C_i \in 0, 1$ indicates a false stop near a wrong object of the target category, a lower CE indicates better instance-level discrimination.

5.2 Performance on Real-World Dataset

We evaluate HEVEN and three baselines (including two non-memory methods and one memory-based method) on the real-world dataset, deploying all methods on the Unitree Go2 quadruped platform. Fig. 7 compares the success rate and end-to-end search time across large (backpacks, laptops), medium (books, hats), and small (cameras, cellphones) targets. The two non-memory methods (i.e., UniGoal [62] and Uninavid [64]) perform poorly on all objects as they rely on real-time visual detection that cannot reliably spot small

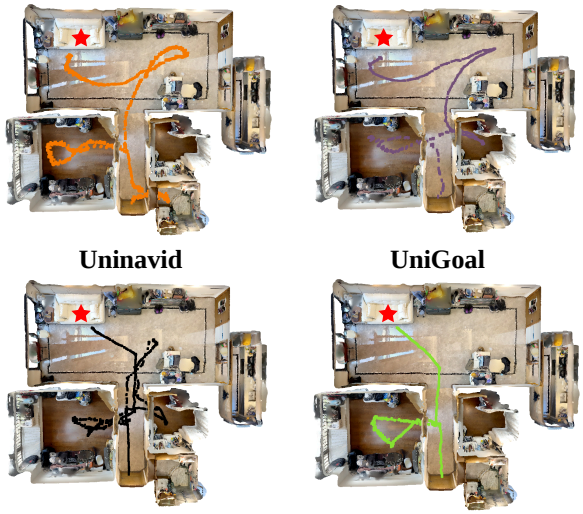

Figure 9: Comparison of navigation trajectories.

daily items in cluttered environments. The memory-based 3DMem [60] achieves moderate success on large objects but degrades on smaller targets with significantly longer search times, because its flat memory presents an unstructured candidate list to the VLM, inflating inference cost and increasing hallucination risk. HEVEN exhibits the highest success rate (over 70%) across all three sizes of objects while achieving the shortest search time (less than 110 s). This is because the SST anchors small objects to stable furniture through the pillar abstraction and organizes the memory of the scene hierarchically, enabling the mobile system to navigate step by step to specific structural landmarks for close-range verification rather than scanning the environment exhaustively.

Specifically, the advantage of HEVEN on the search time stems from two factors: shorter traversal paths and reduced idle waiting. As shown in Fig. 9, UniGoal and Uninavid wander without direction due to the absence of scene memory. 3DMem repeatedly traverses back and forth between distant candidates because its flat list disregards physical distances. HEVEN follows a direct path to the target, as the reachability

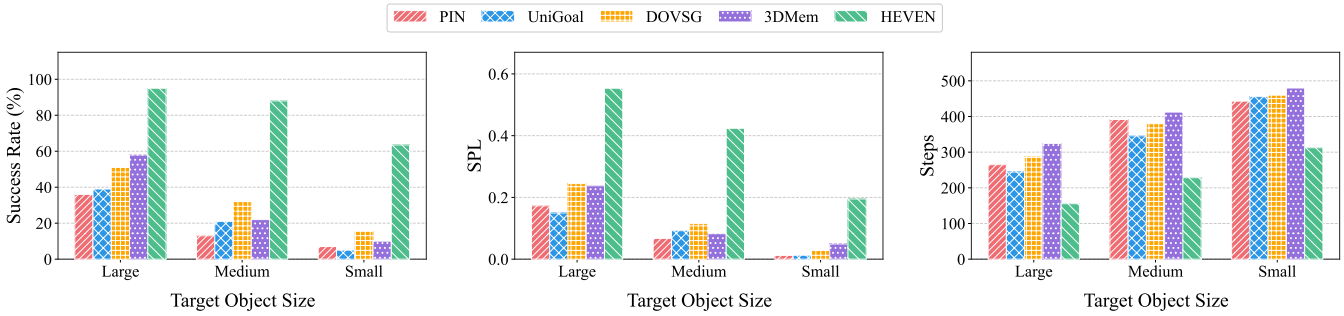

Figure 10: Performance comparison of HEVEN and existing methods on synthetic dataset for different target sizes.

edges in the SST and the cost-aware utility function jointly prioritize nearby high-probability destinations. Fig. 8 further shows the runtime breakdown of HEVEN compared with 3DMem. To ensure a fair comparison, we set the candidates selected by 3DMem to eight to match the eight pillar-level candidates retained in HEVEN's SST pruning. 3DMem operates in a blocking execution style where the mobile system remains waiting during cloud VLM reasoning and re-queries the VLM after each round of eight candidates fails. In contrast, the asynchronous speculative execution of HEVEN pipelines VLM reasoning with physical control, masking the majority of cloud latency behind continuous movement.

Tab. 2 quantifies the resource consumption of HEVEN and baselines on the mobile platform. HEVEN's SST maintains a 15.8 MB memory footprint, an 8.7× reduction compared to 3DMem's 137.2 MB flat memory, as the pillar abstraction compresses raw detections into grouped representations. When the environment changes, the event-driven local update of HEVEN completes in only 0.58 *min* compared to the 24.28 *min* for the full memory reconstruction in 3DMem. On average, for each search episode, HEVEN's hierarchical pruning consumes 7.22*k* tokens with 16.4 *s* of inference time, over 2.4× and 4.4× less than the overhead of the continuous queries in UniGoal and reasoning over the entire flat memory in 3DMem, respectively. Moreover, the inference time of HEVEN is largely hidden behind physical movement, further reducing the perceived waiting time to a few seconds.

5.3 Performance on Synthetic Dataset

We evaluate HEVEN on the multi-room benchmark against two non-memory methods (PIN [5] and UniGoal [62]) and two memory-based methods (3DMem [60] and DOVSG [58]). As shown in Tab. 3, HEVEN achieves a 73.86% success rate with an SPL of 0.35, outperforming the state-of-the-art method DOVSG by 3× in success rate and 4× in path efficiency. Non-memory methods exhibit extremely low success rates (below 16%) and near-zero SPL, as the absence of scene memory reduces navigation to reactive, near-blind search. Memory-based methods perform moderately (up to 24.20% success rate) but their SPL remains below 0.09, indicating that even successful episodes involve highly inefficient traversal. This is because their flat memory structures present the entire unstructured candidate set to the VLM in a single query and disregard the traversal cost between them, resulting in inefficient reasoning and redundant paths. In addition, memory-based methods exhibit the highest category errors (CE above 20%), as their coarse search granularity make the mobile system to stop too far from candidates for reliable instance-level discrimination. HEVEN achieves the lowest distance to goal (3.60 *m*) and the lowest CE (16.16%), as the hierarchical pruning of the SST directs the mobile system to specific pillar-level anchors for close-range verification.

Table 3: Comparison of HEVEN and existing methods on synthetic dataset. "SR", "SPL", "D2G", and "CE" denote success rate, success weighted by path length, distance to goal, and category error, respectively.

Method	SR (%) ↑	SPL ↑	D2G (m) ↓	Steps ↓	CE (%) ↓
None-memory baseline					
PIN [5]	12.60	0.05	10.48	403.97	19.51
UniGoal [62]	15.73	0.06	7.85	397.51	16.98
Memory-based baseline					
3DMem [60]	21.60	0.08	7.72	438.61	20.66
DOVSG [58]	24.20	0.09	8.36	428.40	22.31
HEVEN	**73.86**	**0.35**	**3.60**	**311.32**	**16.16**

Fig. 10 shows the results across large (backpacks, bags, laptops), medium (books, hats, wallets, cameras), and small (cellphones, watches, keys) targets. All baselines degrade sharply as the target size decreases: memory-based methods achieve moderate success on large objects (close to 60% success rate) but drop below 15% on small targets, while non-memory methods fall below 40% even for large objects. In contrast, HEVEN exhibits over 95%, 85%, and 60% success rates for large, medium, and small targets respectively, with consistently the highest SPL and the lowest step count across all size classes. The key reason is that the SST of HEVEN decouples search accuracy from target physical size: regardless of how small the object is, the hierarchical pruning identifies

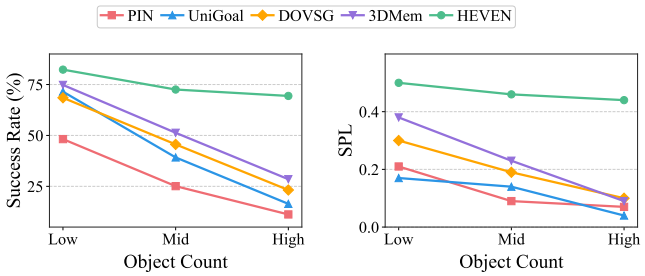

Figure 11: Success rate and SPL under different object count.

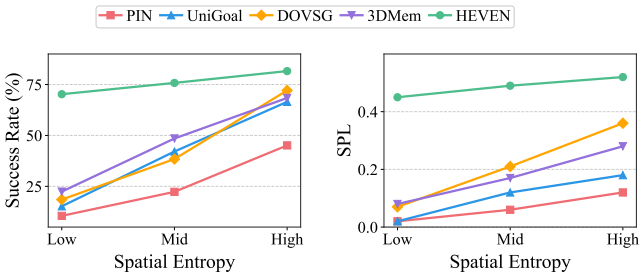

Figure 12: Success rate and SPL under different spatial entropy.

the most likely supporting entity (*e.g.*, a table) and navigates the mobile system to it for close-range verification, rather than relying on the mobile system to detect the small object during a coarse-grained environmental scan.

5.4 Robustness to Scene Complexity

We evaluate HEVEN's robustness against environmental complexity on the synthetic single-room dataset. By isolating two factors: object count and spatial entropy, we evaluate the performance of HEVEN and baselines as scenes become more cluttered or spatially concentrated.

5.4.1 Robustness to Object Count. Fig. 11 compares performance as the number of objects increases. All baseline methods degrade significantly with growing object count. Non-memory methods (PIN, UniGoal) suffer a significant drop in success rates (close to 50%), as their reliance on real-time camera input becomes increasingly ineffective in cluttered environments where the detector is easily distracted. Memory-based methods (3DMem, DOVSG) degrade more gradually but still decline substantially (over 40% drop in success rate and over 0.3 drop in SPL): their flat memory grows proportionally with the number of detected objects, presenting an increasingly massive unstructured candidate list to the VLM that inflates both inference time and hallucination risk. In contrast, HEVEN achieves approximately 70% success rate even under high object count with an SPL above 0.4. This robustness stems from the SST's pillar abstraction: regardless of how many small objects in the scene, they are anchored to a bounded set of supporting entities. The VLM reasons over these pillar-level anchors rather than individual objects, keeping the effective candidate set compact and the reasoning complexity independent of object count.

5.4.2 Robustness to Spatial Entropy. As defined in Sec.4.2.2, lower spatial entropy indicates that objects are more tightly clustered onto fewer furniture pieces, increasing mutual occlusion and spatial ambiguity. Fig.12 evaluates performance of HEVEN and baselines under varying spatial entropy, with object count held constant. Under low spatial entropy, all baseline methods fall below 25% success rate and yield an SPL below 0.15. These methods directly target small objects as search goals, causing the mobile system to approach the scene at a coarse granularity and scan from a distance. When objects are densely packed or partially occluded, this coarse scanning fails to distinguish the target from surrounding clutter. HEVEN maintains ~ 70% success rate while reaching an SPL of 0.45. By using the pillar abstraction as the minimum navigation unit, the SST directs the mobile system to the correct structural landmark regardless of how cluttered it is. Upon arrival, the VLM performs fine-grained target verification at close range, resolving the spatial ambiguity.

5.5 Ablation Study

We conduct ablation studies on the synthetic multi-room dataset to validate two core design choices in HEVEN: the hierarchical depth of the SST and the ToT reasoning strategy. Each experiment isolates one design dimension while keeping all other components fixed.

5.5.1 Impact of SST Depth. Fig. 13 evaluates four SST configurations with increasing depth. Overall, the performance improves consistently as more hierarchical levels are added, confirming that each layer contributes complementary information to the search process. The most significant gain occurs from L0 to L1: introducing a single pillar level raises the success rate from 32% to 55% while reducing the average step count from 460 to around 390. This improvement demonstrates that grouping small objects onto stable entity anchors substantially reduces the candidate set presented to the VLM, alleviating the information overload that causes frequent hallucinations under flat memory. Adding the area level and the room level yields more moderate success rate gains but significantly improves SPL. This is because the area and room levels in SST encode spatial connectivity and traversal cost, enabling the ToT engine to avoid redundant back-and-forth travel between distant areas. Since our current dataset covers scenes up to the multi-room scale, we evaluate SST depth up to three levels. The HEVEN paradigm can be naturally extended to larger environments (e.g., buildings, campuses) by adding higher-level nodes. We leave adaptive depth of SST construction as future work.

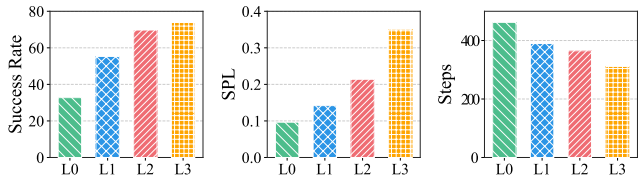

Figure 13: Impact of SST depth on performance. "L0" uses a flat object list as the memory. "L1" introduces hierarchy by grouping small objects onto large entities (pillars). "L2" further groups pillars into functional areas. "L3" denotes the three-level SST used in HEVEN.

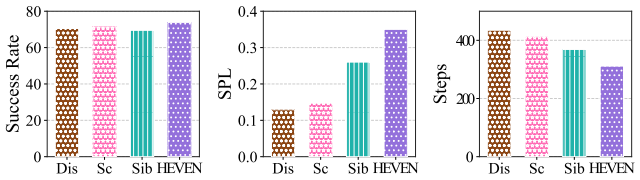

Figure 14: Impact of ToT reasoning strategy on performance. "Dis" reduces the utility function to physical distance only, ignoring semantic relevance. "Sc" uses semantic score only, ignoring traversal cost. "Sib" disables backtracking to higher SST levels, exhausting all sibling nodes under the same parent (area or room) node before proceeding to the next.

5.5.2 Impact of ToT Reasoning Strategy. Fig. 14 shows the performance under different reasoning strategies while keeping the SST fixed. All four variants achieve comparable success rates (over 70%), confirming that the hierarchical memory itself provides sufficient structural information to accurately locate targets. The differences emerge in traversal efficiency and overhead. The "Dis" variant achieves the lowest SPL (0.13) and highest step count (approximately 430). By ignoring semantic relevance, it greedily visits the nearest candidates regardless of their likelihood, wasting steps on improbable locations. The "Sc" variant exhibits similarly poor efficiency, as it frequently guides the mobile system to high-probability but physically distant destinations, incurring excessive travel cost between areas. The "Sib" variant improves the traversal efficiency over the single-factor variants (SPL 0.26), it still underperforms because the system cannot escape a low-utility area once it commits. In contrast, HEVEN dynamically balances traversal cost and semantic relevance through the composite utility function, and adaptively decides whether to continue exploring siblings or backtrack to a different area based on the utility scores. This joint optimization achieves the highest SPL (0.35) with the fewest steps (approximately 310), validating the cost-effectiveness of the ToT reasoning strategy in HEVEN.

6 RELATED WORK

Scene Representations. Traditional geometric maps [48, 8, 47, 20, 33, 51, 15] lack semantic information for language-queried search. While semantic and open-vocabulary mapping [35, 47, 22, 25] grounds visual features in 3D space, maintaining scene knowledge as sparse point clouds or flat object collections scales poorly for small, movable objects. Although 3D Scene Graphs (3DSGs) [46, 23, 58, 44] introduce hierarchy in the scene representation, they target large furniture and leave small items as isolated nodes. In contrast, HEVEN overcomes these limitations by introducing a hierarchical SST, enabling efficient search space pruning rather than reasoning over the entire flat memory.

VLM-Based Navigation. Some works [14, 52, 70, 32, 29] leverage Vision-and-Language Navigation (VLN) instructions for navigation, but such detailed instructions are usually unavailable in real-world applications. Object Navigation (ObjectNav) addresses this using semantic labels via end-to-end or modular approaches. However, end-to-end methods such as reinforcement learning [55, 34] and Vision-Language-Action (VLA) [64, 65, 68] generalize poorly and lack spatial memory, whereas modular systems that leverage explicit maps [13, 5] and VLM-guided exploration [61, 62, 17, 63, 71] rely heavily on real-time perception. Moreover, both of these paradigms are inefficient for search and navigation of small movable objects. Recent memory-based navigation methods [60, 19] leverage VLMs for zero-shot navigation but organize memory as a flat collection. However, as targets become smaller and movable, this unstructured memory can inflates inference costs and hallucination risks. HEVEN resolves these bottlenecks by leveraging the SST to let the VLM hierarchically reason the coarse-to-fine destination with a ToT reasoning engine, effectively utilizing the commonsense of VLM to find the possible locations of the target.

7 CONCLUSION

This paper proposes HEVEN, a system that enables the autonomous mobile system to collaborate with the cloud-based VLM for accurate and efficient small object search and navigation. The key idea is to organize scene memory hierarchically based on spatial containment and support relationships. HEVEN construct the scene memory as a spatial semantic tree and jointly optimizes semantic relevance and travel cost during search and navigation, and pipelines cloud VLM inference with physical control to keep the mobile system in continuous movement. We collect two new datasets across both real-world and synthetic environments. Extensive experiments demonstrate that HEVEN significantly outperforms SOTA baselines in success rate, end-to-end search time, and path efficiency, while substantially reducing memory footprint and VLM inference overhead.

REFERENCES

[1] Alzheimer's Association. 2024. 2024 Alzheimer's disease facts and figures. *Alzheimer's & Dementia*, 20, 5, (May 2024), 3708–3821. doi:10.1002/alz.13809.

[2] Peter Anderson et al. 2018. On evaluation of embodied navigation agents. *arXiv preprint arXiv:1807.06757*.

[3] Jeanne E Arnold, Enzo Ragazzini, Elinor Ochs, and Anthony P Graesch. 2012. Life at home in the twenty-first century: 32 families open their doors. In ISD.

[4] Roshan Ayyalasomayajula, Aditya Arun, Chenfeng Wu, Sanatan Sharma, Abhishek Rajkumar Sethi, Deepak Vasisht, and Dinesh Bharadia. 2020. Deep learning based wireless localization for indoor navigation. In *Proceedings of the 26th Annual International Conference on Mobile Computing and Networking*, 1–14.

[5] Luca Barsellotti, Roberto Bigazzi, Marcella Cornia, Lorenzo Baraldi, and Rita Cucchiara. 2024. Personalized instance-based navigation toward user-specific objects in realistic environments. *Advances in Neural Information Processing Systems*, 37, 11228–11250.

[6] Dhruv Batra, Aaron Gokaslan, Aniruddha Kembhavi, Oleksandr Maksymets, Roozbeh Mottaghi, Manolis Savva, Alexander Toshev, and Erik Wijmans. 2020. Objectnav revisited: on evaluation of embodied agents navigating to objects. *arXiv preprint arXiv:2006.13171*.

[7] Michael Batty. 1974. Spatial entropy. *Geographical analysis*, 6, 1, 1–31.

[8] Berta Bescos, José M Fácil, Javier Civera, and José Neira. 2018. Dynaslam: tracking, mapping, and inpainting in dynamic scenes. *IEEE robotics and automation letters*, 3, 4, 4076–4083.

[9] Kevin Black et al. 2024. \$pi_0: a vision-language-action flow model for general robot control. *arXiv preprint arXiv:2410.24164*.

[10] Robert Bogue. 2016. Growth in e-commerce boosts innovation in the warehouse robot market. *Industrial Robot: An International Journal*, 43, 6, 583–587.

[11] Can Carlak, Bo Yu, Fan Bai, and Z Morley Mao. 2024. State consistent edge-enhanced perception for connected and automated vehicles. In *2024 IEEE 100th Vehicular Technology Conference (VTC2024-Fall)*. IEEE, 1–7.

[12] Angel Chang, Angela Dai, Thomas Funkhouser, Maciej Halber, Matthias Niessner, Manolis Savva, Shuran Song, Andy Zeng, and Yinda Zhang. 2017. Matterport3d: learning from rgb-d data in indoor environments. *arXiv preprint arXiv:1709.06158*.

[13] Devendra Singh Chaplot, Dhiraj Prakashchand Gandhi, Abhinav Gupta, and Russ R Salakhutdinov. 2020. Object goal navigation using goal-oriented semantic exploration. *Advances in Neural Information Processing Systems*, 33, 4247–4258.

[14] Prithvijit Chattopadhyay, Judy Hoffman, Roozbeh Mottaghi, and Aniruddha Kembhavi. 2021. Robustnav: towards benchmarking robustness in embodied navigation. In *Proceedings of the IEEE/CVF International Conference on Computer Vision*, 15691–15700.

[15] Jiahe Cui, Shuyao Shi, Yuze He, Jianwei Niu, Guoliang Xing, and Zhenchao Ouyang. 2024. {Vilam}: infrastructure-assisted 3d visual localization and mapping for autonomous driving. In *21st USENIX Symposium on Networked Systems Design and Implementation (NSDI 24)*, 1831–1845.

[16] Zipeng Fu, Tony Z Zhao, and Chelsea Finn. 2024. Mobile aloha: learning bimanual mobile manipulation with low-cost whole-body teleoperation. *arXiv preprint arXiv:2401.02117*.

[17] Samir Yitzhak Gadre, Mitchell Wortsman, Gabriel Ilharco, Ludwig Schmidt, and Shuran Song. 2023. Cows on pasture: baselines and benchmarks for language-driven zero-shot object navigation. In *Proceedings of the IEEE/CVF Conference on Computer Vision and Pattern Recognition*, 23171–23181.

[18] Grand View Research. 2024. Service Robotics Market Size, Share & Trends Analysis Report by Application (Professional, Personal), by End Use (Defense, Field, Medical, Transportation and Logistics, Construction), by Region, and Segment Forecasts, 2024–2030. Tech. rep. 978-1-68038-040-8. Accessed: 2026-03-14. Grand View Research.

[19] Qiao Gu et al. 2024. Conceptgraphs: open-vocabulary 3d scene graphs for perception and planning. In *2024 IEEE International Conference on Robotics and Automation (ICRA)*. IEEE, 5021–5028.

[20] Wolfgang Hess, Damon Kohler, Holger Rapp, and Daniel Andor. 2016. Real-time loop closure in 2d lidar slam. In *2016 IEEE international conference on robotics and automation (ICRA)*. IEEE, 1271–1278.

[21] Jane Holland, Liz Kingston, Conor McCarthy, Eddie Armstrong, Peter O'dwyer, Fionn Merz, and Mark McConnell. 2021. Service robots in the healthcare sector. *Robotics*, 10, 1, 47.

[22] Chenguang Huang, Oier Mees, Andy Zeng, and Wolfram Burgard. 2023. Visual language maps for robot navigation. In *2023 IEEE International Conference on Robotics and Automation (ICRA)*. IEEE, 10608–10615.

[23] Nathan Hughes, Yun Chang, and Luca Carlone. 2022. Hydra: a real-time spatial perception system for 3d scene graph construction and optimization. *arXiv preprint arXiv:2201.13360*.

[24] Intel Corporation. 2018. Intel RealSense depth camera D435i. https://www.realsenseai.com/products/depth-camera-d435i/. Accessed: 2026-03-11. (2018).

[25] Krishna Murthy Jatavallabhula et al. 2023. Conceptfusion: open-set multimodal 3d mapping. *arXiv preprint arXiv:2302.07241*.

[26] Rajat Kumar Jenamani et al. 2025. Feast: a flexible mealtime-assistance system towards in-the-wild personalization. *arXiv:2506.14968*.

[27] Alexander Kirillov et al. 2023. Segment anything. In *Proceedings of the IEEE/CVF international conference on computer vision*, 4015–4026.

[28] Jacob Krantz, Stefan Lee, Jitendra Malik, Dhruv Batra, and Devendra Singh Chaplot. 2022. Instance-specific image goal navigation: training embodied agents to find object instances. *arXiv preprint arXiv:2211.15876*.

[29] Bingqian Lin, Yunshuang Nie, Ziming Wei, Jiaqi Chen, Shikui Ma, Jianhua Han, Hang Xu, Xiaojun Chang, and Xiaodan Liang. 2025. Navcot: boosting llm-based vision-and-language navigation via learning disentangled reasoning. *IEEE Transactions on Pattern Analysis and Machine Intelligence*.

[30] Peiqi Liu, Yaswanth Orru, Jay Vakil, Chris Paxton, Nur Muhammad Mahi Shafiullah, and Lerrel Pinto. 2024. Ok-robot: what really matters in integrating open-knowledge models for robotics. *arXiv preprint arXiv:2401.12202*.

[31] Shilong Liu et al. 2024. Grounding dino: marrying dino with grounded pre-training for open-set object detection. In *European conference on computer vision*. Springer, 38–55.

[32] Yuxing Long, Xiaoqi Li, Wenzhe Cai, and Hao Dong. 2024. Discuss before moving: visual language navigation via multi-expert discussions. In *2024 IEEE International Conference on Robotics and Automation (ICRA)*. IEEE, 17380–17387.

[33] Steve Macenski, Francisco Martín, Ruffin White, and Jonatan Ginés Clavero. 2020. The marathon 2: a navigation system. In *2020 IEEE/RSJ International Conference on Intelligent Robots and Systems (IROS)*. IEEE, 2718–2725.

[34] Arjun Majumdar, Gunjan Aggarwal, Bhavika Devnani, Judy Hoffman, and Dhruv Batra. 2022. Zson: zero-shot object-goal navigation using multimodal goal embeddings. *Advances in Neural Information Processing Systems*, 35, 32340–32352.

[35] John McCormac, Ankur Handa, Andrew Davison, and Stefan Leutenegger. 2017. Semanticfusion: dense 3d semantic mapping with convolutional neural networks. In *2017 IEEE International Conference on Robotics and automation (ICRA)*. IEEE, 4628–4635.

[36] NVIDIA. 2022. NVIDIA Isaac Sim: a scalable robotics simulation and synthetic data generation platform. https://developer.nvidia.com/isaac/sim. Accessed: 2026-03-11. (2022).

[37] NVIDIA. 2022. NVIDIA Jetson AGX Orin series. https://www.nvidia.com/en-us/autonomous-machines/embedded-systems/jetson-orin/. Accessed: 2026-03-11. (2022).

[38] OpenAI. 2024. Hello GPT-4o. https://openai.com/index/hello-gpt-4o/. Accessed: 2026-03-11. (2024).

[39] Pixie Technology. 2017. Lost and found: the average American spends 2.5 days each year looking for lost items, collectively costing U.S. households $2.7 billion annually in replacement costs. PR Newswire. Survey of 1,700+ participants conducted by Survey Sampling International, October 2016. (May 2017).

[40] Anne Margriet Pot, Bernadette M Willemse, and Sarah Horjus. 2012. A pilot study on the use of tracking technology: feasibility, acceptability, and benefits for people in early stages of dementia and their informal caregivers. *Aging & mental health*, 16, 1, 127–134.

[41] Alec Radford et al. 2021. Learning transferable visual models from natural language supervision. In *International conference on machine learning*. PmLR, 8748–8763.

[42] Alexander Raistrick et al. 2024. Infinigen indoors: photorealistic indoor scenes using procedural generation. In *Proceedings of the IEEE/CVF Conference on Computer Vision and Pattern Recognition*, 21783–21794.

[43] Santhosh K Ramakrishnan et al. 2021. Habitat-matterport 3d dataset (hm3d): 1000 large-scale 3d environments for embodied ai. *arXiv preprint arXiv:2109.08238*.

[44] Krishan Rana, Jesse Haviland, Sourav Garg, Jad Abou-Chakra, Ian Reid, and Niko Suenderhauf. 2023. Sayplan: grounding large language models using 3d scene graphs for scalable robot task planning. *arXiv preprint arXiv:2307.06135*.

[45] Tianhe Ren et al. 2024. Grounded sam: assembling open-world models for diverse visual tasks. *ArXiv*, abs/2401.14159. https://api.semanticscholar.org/CorpusID:267212047.

[46] Antoni Rosinol, Marcus Abate, Yun Chang, and Luca Carlone. 2020. Kimera: an open-source library for real-time metric-semantic localization and mapping. In *2020 IEEE international conference on robotics and automation (ICRA)*. IEEE, 1689–1696.

[47] Martin Runz, Maud Buffier, and Lourdes Agapito. 2018. Maskfusion: real-time recognition, tracking and reconstruction of multiple moving objects. In *2018 IEEE international symposium on mixed and augmented reality (ISMAR)*. IEEE, 10–20.

[48] Renato F Salas-Moreno, Richard A Newcombe, Hauke Strasdat, Paul HJ Kelly, and Andrew J Davison. 2013. Slam++: simultaneous localisation and mapping at the level of objects. In *Proceedings of the IEEE conference on computer vision and pattern recognition*, 1352–1359.

[49] Dhruv Shah, Błażej Osiński, Sergey Levine, et al. 2023. Lm-nav: robotic navigation with large pre-trained models of language, vision, and action. In *Conference on robot learning*. pmlr, 492–504.

[50] Shuyao Shi, Jiahe Cui, Zhehao Jiang, Zhenyu Yan, Guoliang Xing, Jianwei Niu, and Zhenchao Ouyang. 2022. Vips: real-time perception fusion for infrastructure-assisted autonomous driving. In *Proceedings of the 28th annual international conference on mobile computing and networking*, 133–146.

[51] Sebastian Thrun. 2002. Probabilistic robotics. *Communications of the ACM*, 45, 3, 52–57.

[52] Joanne Truong, Sonia Chernova, and Dhruv Batra. 2021. Bi-directional domain adaptation for sim2real transfer of embodied navigation agents. *IEEE Robotics and Automation Letters*, 6, 2, 2634–2641.

[53] Unitree Robotics. 2023. Unitree Go2: ai robot dog. https://www.unitree.com/go2/. Accessed: 2026-03-11. (2023).

[54] Haoming Wang, Qiyao Xue, Weichen Liu, and Wei Gao. 2026. Mosaicthinker: on-device visual spatial reasoning for embodied ai via iterative construction of space representation. *arXiv preprint arXiv:2602.07082*.

[55] Erik Wijmans, Abhishek Kadian, Ari Morcos, Stefan Lee, Irfan Essa, Devi Parikh, Manolis Savva, and Dhruv Batra. 2019. Dd-ppo: learning near-perfect pointgoal navigators from 2.5 billion frames. *arXiv preprint arXiv:1911.00357*.

[56] Jimmy Wu, William Chong, Robert Holmberg, Aaditya Prasad, Yihuai Gao, Oussama Khatib, Shuran Song, Szymon Rusinkiewicz, and Jeannette Bohg. 2024. Tidybot++: an open-source holonomic mobile manipulator for robot learning. *arXiv preprint arXiv:2412.10447*.

[57] Brian Yamauchi. 1997. A frontier-based approach for autonomous exploration. In *Proceedings 1997 IEEE International Symposium on Computational Intelligence in Robotics and Automation CIRA'97.'Towards New Computational Principles for Robotics and Automation'*. IEEE, 146–151.

[58] Zhijie Yan, Shufei Li, Zuoxu Wang, Lixiu Wu, Han Wang, Jun Zhu, Lijiang Chen, and Jihong Liu. 2025. Dynamic open-vocabulary 3d scene graphs for long-term language-guided mobile manipulation. *IEEE Robotics and Automation Letters*.

[59] Guang-Zhong Yang et al. 2020. Combating covid-19—the role of robotics in managing public health and infectious diseases. (2020).

[60] Yuncong Yang, Han Yang, Jiachen Zhou, Peihao Chen, Hongxin Zhang, Yilun Du, and Chuang Gan. 2025. 3d-mem: 3d scene memory for embodied exploration and reasoning. In *Proceedings of the Computer Vision and Pattern Recognition Conference*, 17294–17303.

[61] Hang Yin, Xiuwei Xu, Zhenyu Wu, Jie Zhou, and Jiwen Lu. 2024. Sg-nav: online 3d scene graph prompting for llm-based zero-shot object navigation. *Advances in neural information processing systems*, 37, 5285–5307.

[62] Hang Yin, Xiuwei Xu, Linqing Zhao, Ziwei Wang, Jie Zhou, and Jiwen Lu. 2025. Unigoal: towards universal zero-shot goal-oriented navigation. In *Proceedings of the IEEE/CVF Conference on Computer Vision and Pattern Recognition*, 19057–19066.

[63] Bangguo Yu, Hamidreza Kasaei, and Ming Cao. 2023. L3mvn: leveraging large language models for visual target navigation. In *2023 IEEE/RSJ International Conference on Intelligent Robots and Systems (IROS)*. IEEE, 3554–3560.

[64] Jiazhao Zhang, Kunyu Wang, Shaoan Wang, Minghan Li, Haoran Liu, Songlin Wei, Zhongyuan Wang, Zhizheng Zhang, and He Wang. 2024. Uni-navid: a video-based vision-language-action model for unifying embodied navigation tasks. *arXiv preprint arXiv:2412.06224*.

[65] Jiazhao Zhang, Kunyu Wang, Rongtao Xu, Gengze Zhou, Yicong Hong, Xiaomeng Fang, Qi Wu, Zhizheng Zhang, and He Wang. 2024. Navid: video-based vlm plans the next step for vision-and-language navigation. *arXiv preprint arXiv:2402.15852*.

[66] Qingzhao Zhang, Xumiao Zhang, Ruiyang Zhu, Fan Bai, Mohammad Naserian, and Z Morley Mao. 2023. Robust real-time multi-vehicle collaboration on asynchronous sensors. In *Proceedings of the 29th Annual International Conference on Mobile Computing and Networking*, 1–15.

[67] Wuyang Zhang, Zhezhi He, Luyang Liu, Zhenhua Jia, Yunxin Liu, Marco Gruteser, Dipankar Raychaudhuri, and Yanyong Zhang. 2021. Elf: accelerate high-resolution mobile deep vision with content-aware parallel offloading. In *Proceedings of the 27th Annual International Conference on Mobile Computing and Networking*, 201–214.

[68] Duo Zheng, Shijia Huang, Lin Zhao, Yiwu Zhong, and Liwei Wang. 2024. Towards learning a generalist model for embodied navigation. In *Proceedings of the IEEE/CVF Conference on Computer Vision and Pattern Recognition*, 13624–13634.

[69] Anfu Zhou, Shaoqing Xu, Song Wang, Jingqi Huang, Shaoyuan Yang, Teng Wei, Xinyu Zhang, and Huadong Ma. 2019. Robot navigation

in radio beam space: leveraging robotic intelligence for seamless mmwave network coverage. In *Proceedings of the Twentieth ACM International Symposium on Mobile Ad Hoc Networking and Computing*, 161–170.

[70] Gengze Zhou, Yicong Hong, and Qi Wu. 2024. Navgpt: explicit reasoning in vision-and-language navigation with large language models. In *Proceedings of the AAAI Conference on Artificial Intelligence* number 7. Vol. 38, 7641–7649.

[71] Kaiwen Zhou, Kaizhi Zheng, Connor Pryor, Yilin Shen, Hongxia Jin, Lise Getoor, and Xin Eric Wang. 2023. Esc: exploration with soft commonsense constraints for zero-shot object navigation. In *International Conference on Machine Learning*. PMLR, 42829–42842.